

Numerical Analysis of Optimized Coherent Control Pulses

P. Karbach,¹ S. Pasini,¹ and G. S. Uhrig¹

¹*Lehrstuhl für Theoretische Physik I, Technische Universität Dortmund,
Otto-Hahn Straße 4, 44221 Dortmund, Germany*

(Dated: November 1, 2018)

Numerically we simulate the effect of optimized coherent control pulses with a finite duration on a qubit in a bath of spins. The pulses of finite duration are compared with ideal instantaneous pulses. In particular, we show that properly designed short pulses can approximate ideal instantaneous pulses up to a certain order in the shortness of the pulse. We provide examples of such pulses, quantify the discrepancy from the ideal case and compare their effect for various ranges of the coupling constants.

PACS numbers: 03.67.Lx, 03.67.Pp, 75.40.Mg, 76.60.-k

I. INTRODUCTION

The coherent control of quantum systems continues to be a topic of great interest. The possibility of maintaining a spin in a coherent state is of extreme importance in fields of application like nuclear magnetic resonance (NMR) or the manipulation of quantum dots. In particular for quantum information processing, a long coherence time of the qubit is an indispensable prerequisite for its realization.

A quantum bit (henceforth: qubit) is a two-level system which is conveniently regarded as a spin $S = 1/2$. Operations on qubits to change or to correct their state are performed through quantum gates. Their effect on the density matrix of the qubit can be described as a rotation in the Bloch sphere. Experimentally, they often can be obtained by the application of electromagnetic pulses. A 1-qubit gate is generally a single rotation about a given axis \vec{a} in spin space. The angle of rotation classifies the type of the pulse. For instance a π pulse rotates the spin by 180° . These pulses find a wide range of applications in dynamical decoupling [1, 2, 3, 4, 5, 6, 7] and in NMR [8, 9] where also $\pi/2$ pulses are crucial. In quantum information processing the $\pi/2$ pulse in combination with a π pulse realizes the important Hadamard gate.

The idea of dynamical decoupling (DD) [1, 2, 3, 4, 5, 6, 7] has been developed from the spin echo technique in NMR [10, 11, 12]. DD aims at decoupling the qubit from the environment by means of the application of appropriate pulse sequences. From a theoretical point of view the topic has been widely studied and many different sequences of pulses have been proposed. Among these we recall the series of periodic equidistant π pulses, called bang-bang control (BB) [1, 2], the periodically iterated 2-pulse sequence according to Carr/Purcell and Meiboom/Gill (CPMG) [8, 11, 12], the concatenated sequence (CDD) proposed by Khodjasteh and Lidar [13, 14] as well as the fully optimized sequence (UDD) derived by one of the authors [7, 15].

Experimentally, the spin echo and the CPMG sequence are standard in NMR [8]. To our knowledge, other sequences have not yet been tested. In realizations of qubits

on the basis of semiconductor technology so far only the spin echo technique has been implemented [16, 17, 18]. But computations for quantum dot systems show that more elaborate pulse sequences are very likely to be useful in suppressing decoherence, see for instance [5, 6, 19].

Most theoretical examples (for exceptions see Ref. [13, 14]) reported so far have the limitation that the pulses are assumed to be ideal. This means that the pulses are considered to be instantaneous and infinitely strong in the sense of a δ peak. In this case, one is allowed to ignore the effect of the bath, inducing the decoherence, during the action of the pulse because the coupling to the bath is negligible relative to the amplitude of the δ pulse. Hence the rotation due to the pulse can be viewed to be completely separate from the free evolution of the system, qubit and bath, without pulse.

If the pulse has a finite duration (τ_p) so that its time of application is comparable with the characteristic time scales of the bath, the separation between evolution due to the pulse and evolution of the undriven system is not valid anymore. If we suppose that the duration τ_p is still small an expansion in τ_p about the limit of a δ pulse is appropriate. The proposed scenario [20] establishes an equivalence, up to corrections expanded in a series in τ_p , between the real pulse and an ideal δ pulse at some intermediate instant τ_s with $0 < \tau_s < \tau_p$, see Figs. 1, 2, and 3. Before and after the ersatz pulse at τ_s , the free evolution of the system, qubit and bath, without pulse takes place.

The corrections expanded in powers of τ_p depend also on the shape of the pulse; so one can aim at making them vanish or at minimizing them by shaping the pulses skillfully. This is the route that we established previously [20] analytically by the expansion in τ_p . In the present work, we demonstrate numerically that the higher order corrections neglected in the analytical calculations are indeed negligible. Thereby, we have shown not only the validity of the previous analytic calculation but we have also demonstrated that the real performance of the proposed pulses is advantageous.

We draw the readers' attention to the fact that shaped pulses have been introduced in NMR previously, see for instance the Refs. 21, 22, 23, 24, 25, 26, 27 and Ref. 9

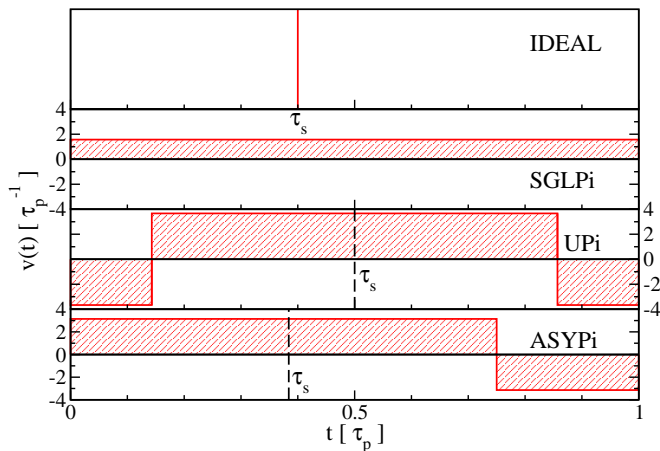


Figure 1: (Color online) Examples of π pulses implemented in the simulations. The ideal pulse is given by a δ peak operating at the instant τ_s . SGLPi is the standard pulse of constant amplitude without optimization of the pulse shape. For details see Table I.

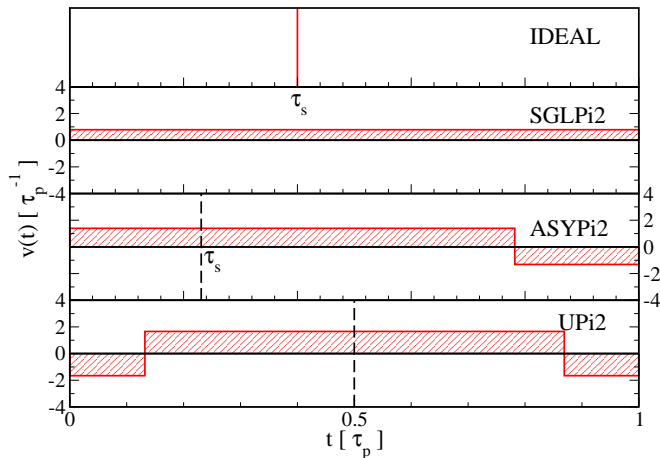


Figure 2: (Color online) Examples of $\pi/2$ pulses implemented in the simulations. The ideal pulse is given by a δ peak operating at the instant τ_s . SGLPi2 is the standard pulse of constant amplitude without optimization of the pulse shape. For details see Table II.

for an overview in the field of quantum information. But the goals of these investigations were different from ours even though it turned out that for π pulses certain shapes with $\tau_s = \tau_p/2$ happen to coincide [20].

The paper is organized as follows. In Sect. II we briefly recall the analytical arguments for the expansion in powers of τ_p ; especially the expressions for the first and second order corrections are given. Then we introduce a quantity to measure the deviation of the real pulse from the ideal pulse and compute this deviation analytically. Moreover, we relate the two parameters of the model to the experimental situation in various realizations of qubits. In Sect. III the spin Hamiltonian is introduced

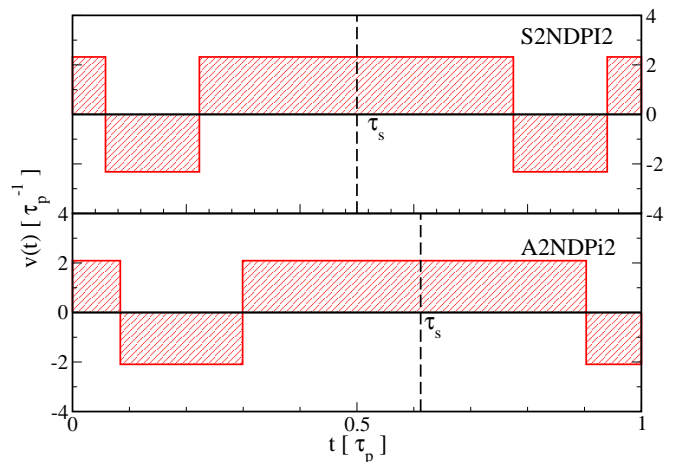


Figure 3: (Color online) Examples of $\pi/2$ pulses for which also some of the second order corrections vanish, namely $\eta_{21} = 0$ and $\eta_{22} = 0$ (see main text). For details see Table II.

which serves as our system of a qubit coupled to a decoherence bath. For this model we compute the deviation between real and ideal pulse analytically and numerically. The experimentally relevant ranges of parameters are estimated. The numerical results are discussed in Sect. IV for π and for $\pi/2$ pulses. Finally, in Sect. V we draw our conclusions.

II. THEORETICAL PREDICTIONS

A. First and second order corrections

In order to disentangle the actual pulse and the free evolution of the system we proceed as follows. The total unitary time evolution during the real pulse is split into the time evolution of the system alone and of the pulse alone which is taken to occur at τ_s within the interval $[0, \tau_p]$, see Ref. 20. The time evolution of the system alone is taken to occur before and after the evolution due to the pulse. The evolution due to the pulse is multiplied additionally by corrections coming from the non-commutation of the Hamiltonians of the pulse and of the system. They can be expanded in a series in τ_p . It is important to stress that this technique does not aim at eliminating the coupling between the qubit and the bath completely, but only at separating the effect of the pulse from that of bath. The coupling between the qubit and the bath remains active during the free evolution of the system.

To be explicit, we consider the following general Hamiltonian

$$H_{\text{tot}} = H + H_0(t), \quad (1)$$

where the Hamiltonian H of the qubit coupled to the

bath is

$$H = H_b + \lambda A \sigma_z, \quad (2)$$

where H_b is a completely general bath and A a completely general coupling operator acting on the bath. The Pauli matrices represent operators acting on the qubit. The internal energy scale of H_b shall be denoted by ω_b while λ is the coupling constant between qubit and bath.

Note that we assume only a coupling along the z direction. Hence the model contains only dephasing, i.e., a finite T_2 . No spin flips are possible so that $T_1 = \infty$. Though this represents a restriction it is well justified for large magnetic fields along z so that all other couplings average out in the rotating-frame approximation.

The Hamiltonian of the pulse is denoted by H_0

$$H_0(t) = v(t)\sigma_y, \quad (3)$$

representing a rotation around the y axis. The pulse shape is given by the function $v(t)$. Note that H_0 and H do not commute implying that the unitary time evolution $U(\tau_p, 0)$ during the application of a pulse is a non-trivial quantity.

Splitting the time evolution $U(\tau_p, 0)$ into the time evolutions during two intervals, $U(\tau_p, \tau_s)$ and $U(\tau_s, 0)$, and formally solving the Schrödinger equation for each of them with a suitable ansatz we eventually obtain (for details see Refs. 20)

$$\begin{aligned} U_p(\tau_p, 0) &= \mathbb{T} \left\{ e^{-i \int_0^{\tau_p} H_{tot}(t) dt} \right\} \\ &= e^{-i(\tau_p - \tau_s)H} e^{-i\sigma_y \int_{\tau_s}^{\tau_p} v(t) dt} U_F(\tau_p, 0) \\ &\quad e^{-i\sigma_y \int_0^{\tau_s} v(t) dt} e^{-i\tau_s H}. \end{aligned} \quad (4)$$

where $U_F(\tau_p, 0)$ represents the correction term. Without any correction, i.e., for $U_F(\tau_p, 0) = 1$, the two exponentials of the pulse can be combined in the middle of the right hand side of Eq. (4) so that the unitary operator of the ideal pulse occurs

$$U_p(\tau_p, 0) = e^{-i(\tau_p - \tau_s)H} e^{-i\sigma_y \int_0^{\tau_p} v(t) dt} e^{-i\tau_s H}. \quad (5)$$

The correction is expanded in a series in powers of τ_p

$$U_F(\tau_p, 0) = \exp(-i(\eta^{(1)} + \eta^{(2)} + \dots)) \quad (6)$$

where $\eta^{(j)}$ is the term of order τ_p^j . We obtained [20]

$$\eta^{(1)} = (\eta_{11}\sigma_x + \eta_{12}\sigma_z)\lambda A \quad (7a)$$

$$\eta^{(2)} = i(\eta_{21}\sigma_x + \eta_{22}\sigma_z)\lambda[H_b, A] + \eta_{23}\sigma_y\lambda^2 A^2. \quad (7b)$$

Note that $[H_b, A]$ is of the order of ω_b so that the corresponding term is indeed of order $\lambda\omega_b\tau_p^2$, thus of second order in τ_p^2 . This becomes manifest in the explicit inte-

τ_s	amplitude(s)	τ_i	$\eta^{(2)}$
SGLPi			
1/2	$\pi/2$	-	-
UPi			
1/2	$\pm 7\pi/6$	1/7 6/7	0.04401 0 0.12295
ASYPi			
0.34085	$\pm 13\pi/6$	3/4	-0.00653 -0.14783 0.18087

Table I: Overview of the π pulses implemented in the simulations. UPi and SGLPi are symmetric pulses ($\tau_s = \tau_p/2$). The switching instants τ_i and the amplitudes are given in units of τ_p and $1/\tau_p$, respectively. The column $\eta^{(2)}$ refers from top to bottom to the coefficients $\eta_{21}, \eta_{22}, \eta_{23}$ in units of τ_p^2 , see Eq. (7)

gral equations for the coefficients η_{ij}

$$\eta_{11} = (\tau_p - \tau_s) \sin \psi_{\tau_p} + \tau_s \sin \psi_0 - \int_0^{\tau_p} \sin \psi_t dt \quad (8a)$$

$$\eta_{12} = (\tau_p - \tau_s) \cos \psi_{\tau_p} + \tau_s \cos \psi_0 - \int_0^{\tau_p} \cos \psi_t dt \quad (8b)$$

$$\begin{aligned} \eta_{21} &= \frac{(\tau_p - \tau_s)^2}{2} \sin \psi_{\tau_p} - \frac{\tau_s^2}{2} \sin \psi_0 \\ &\quad - \int_0^{\tau_p} \Delta t \sin \psi_t dt \end{aligned} \quad (8c)$$

$$\begin{aligned} \eta_{22} &= -\frac{(\tau_p - \tau_s)^2}{2} \cos \psi_{\tau_p} + \frac{\tau_s^2}{2} \cos \psi_0 \\ &\quad + \int_0^{\tau_p} \Delta t \cos \psi_t dt \end{aligned} \quad (8d)$$

$$\begin{aligned} \eta_{23} &= (\tau_p - \tau_s)\tau_s \sin \theta - \tau_s \int_0^{\tau_p} \sin(\psi_t - \psi_0) dt \\ &\quad - (\tau_p - \tau_s) \int_0^{\tau_p} \sin(\psi_{\tau_p} - \psi_t) dt \\ &\quad + \frac{1}{2} \iint_0^{\tau_p} \sin(\psi_{t_1} - \psi_{t_2}) \text{sgn}(t_1 - t_2) dt_1 dt_2, \end{aligned} \quad (8e)$$

where $\psi_t = 2 \int_{\tau_s}^t v(t') dt'$, $\Delta t = t - \tau_s$, and $\theta = \psi_{\tau_p} - \psi_0$ is the area under the amplitude of the pulse. The angle θ represents the total angle of rotation of the qubit's spin under the action of the pulse.

The function $v(t)$ and the instant τ_s are the free variables which can be fine-tuned to ideally make the coefficients η_{ij} vanish or at least to minimize their moduli. In Fig. 1 examples of piecewise constant pulses for $\theta = \pi$ are reported. The pulse SGLPi is the standard pulse of constant amplitude which has finite first and second order corrections. The pulses UPi and ASYPi are chosen such that their first order correction $\eta^{(1)}$ vanishes. Their second order correction $\eta^{(2)}$ does not vanish. We have

proven previously that $\eta^{(2)}$ cannot be made vanish for a π pulse. [20]. For quantitative details, see Tab. I.

τ_s	amplitude(s)	τ_i	$\eta^{(2)}$
SGLPi2			
1/2	$\pi/4$	-	-
UPi2			
1/2	± 1.65765	0.13155 0.86845	-0.01305 0 0.05151
ASYPi2			
0.23128	± 1.39116	0.78220	-0.01279 -0.05691 0.88990
S2NDPi2			
1/2	± 2.31993	0.05848 0.22384 0.77616 0.94152	0 0 ± 0.01335
A2NDPi2			
0.61218	± 2.09429	0.08361 0.29828 0.90217	0 0 ± 0.01659

Table II: Overview of the $\pi/2$ pulses implemented in the simulation. UPi2, SGLPi2, and S2NDPi2 are symmetric pulses ($\tau_s = \tau_p/2$). The switching instants τ_i and the amplitudes are given in units of τ_p and $1/\tau_p$, respectively. The column $\eta^{(2)}$ refers from top to bottom to the coefficients η_{21} , η_{22} , η_{23} in units of τ_p^2 , see Eq. (7)

In analogy, Fig. 2 depicts examples of piecewise constant pulses for $\theta = \pi/2$. The pulse SGLPi2 is the standard pulse of constant amplitude which has finite first and second order corrections. The pulses UPi2 and ASYPi2 are chosen such that their first order correction $\eta^{(1)}$ vanishes. Their second order correction $\eta^{(2)}$ does not vanish. For the quantitative details, we refer the reader to Tab. II.

The pulses S2ND2 and A2NDPi2 are plotted in Fig. 3. They are chosen such that their first order correction $\eta^{(1)}$ and the second order coefficients η_{21} and η_{22} vanish. We were not able to find a solution which has additionally $\eta_{23} = 0$. But we have not succeeded in proving the impossibility of finding such a solution either. For the quantitative details, we refer the reader to Tab. II.

B. Measure of deviation

The above results represent the analytical finding that we intend to check numerically. In order to do so we need a measure of how well the real pulse approximates the ideal instantaneous one. We define the operator difference $\Delta := U_p^i - U_p^r$ which quantifies the distance of

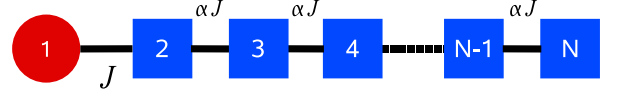


Figure 4: (Color online) Sketch of the spin chain representing qubit and spin bath. The qubit 1 is coupled to the spin 2 of the chain. The coupling between qubit and the spin bath is given by J while the internal exchange coupling within the chain is αJ .

the ideal time evolution (U_p^i) from the real one (U_p^r). To capture this distance by a single number we define the norm

$$d := \sqrt{\max \{\text{Eigenvalues}(\Delta^\dagger \Delta)\}}. \quad (9)$$

For a pulse of angle θ , the ideal pulse reads

$$U_p^i = e^{-i(\tau_p - \tau_s)H} e^{-i\frac{\theta}{2}\sigma_y} e^{-i\tau_s H} \quad (10)$$

while the real pulse is given by

$$U_p^r = e^{-i(\tau_p - \tau_s)H} e^{-i\frac{\psi\tau_p}{2}\sigma_y} U_F(\tau_p, 0) e^{i\frac{\psi_0}{2}\sigma_y} e^{-i\tau_s H}, \quad (11)$$

such that

$$\Delta = e^{-i(\tau_p - \tau_s)H} e^{-i\frac{\psi\tau_p}{2}\sigma_y} (\mathbb{1} - U_F(\tau_p, 0)) e^{i\frac{\psi_0}{2}\sigma_y} e^{-i\tau_s H}. \quad (12)$$

This implies

$$\Delta^\dagger \Delta = \tilde{U}^\dagger (\mathbb{1} - U_F^\dagger(\tau_p, 0)) (\mathbb{1} - U_F(\tau_p, 0)) \tilde{U}, \quad (13)$$

where $\tilde{U} = e^{-i\frac{\psi_0}{2}\sigma_y} e^{-i\tau_s H}$ is a unitary operator which leaves the eigenvalues of the product $(\mathbb{1} - U_F^\dagger(\tau_p, 0))(\mathbb{1} - U_F(\tau_p, 0))$ unaffected.

Next, we expand U_F in τ_p . If the leading order is $\eta^{(1)}$ we have $U_F \approx \mathbb{1} - i\eta^{(1)} + \mathcal{O}(\tau_p^2)$ whence

$$d = \sqrt{\max \{\text{Eigenvalues}(\eta^{(1)}\eta^{(1)})\} + \mathcal{O}(\tau_p^3)}. \quad (14)$$

If the leading order is $\eta^{(2)}$ we have $U_F \approx \mathbb{1} - i\eta^{(2)} + \mathcal{O}(\tau_p^3)$ whence

$$d = \sqrt{\max \{\text{Eigenvalues}(\eta^{(2)}\eta^{(2)})\} + \mathcal{O}(\tau_p^5)}. \quad (15)$$

We deduce that in the case of finite first order $\eta^{(1)} \neq 0$ one has $d = \mathcal{O}(\tau_p)$ while for vanishing first order, but finite second order $\eta^{(2)} \neq 0$ one has $d = \mathcal{O}(\tau_p^2)$.

III. THE SPIN CHAIN AS DECOHERENCE BATH

A. The Model

The formulae (14,15) for d hold for any Hamiltonian that can be expressed in the form (2). Next, we specify

the model we investigate numerically. It is a spin chain of N spins where the first spin ($\vec{\sigma}$) represents the qubit, see Fig. 4. The Hamiltonian considered is given by

$$H_s = J\tilde{\sigma}_z\sigma_z^{(2)} + \alpha J \sum_{i=2}^N \vec{\sigma}^{(i)} \cdot \vec{\sigma}^{(i+1)}. \quad (16)$$

Obviously, this Hamiltonian is an example for the most general dephasing Hamiltonian (2). In (16) the bath is a bath of spins and the coupling between bath and qubit is quantified by J ; hence we have $\lambda = J$. The internal energy scale of the bath ω_b equals αJ in (16).

In order to apply our general results (14,15) we have to compute $\eta^{(2)}$ for the specific case of the spin Hamiltonian (16). The bath operator A in (2) consists only of the z component of the second spin. Hence one has $A^2 = \mathbb{1}$.

The other term in (7b) comprises $[H_b, A]$. For (16) this commutator contains only the second and the third spin. Hence we anticipate that the numerical results will not show any significant size dependence in the regime where the expansion in τ_p is valid, i.e., for low values of λ and ω_b which translates to low values of J . Explicitly we find for $\eta^{(2)}$

$$\eta^{(2)} = -2J^2\alpha(\eta_{21}\tilde{\sigma}_x + \eta_{22}\tilde{\sigma}_z)(\vec{\sigma}^{(2)} \times \vec{\sigma}^{(3)})_z + \eta_{23}J^2\tilde{\sigma}_y, \quad (17)$$

where $(\)_z$ stands for the z component. Because only three spins occur, it is a basic exercise to determine for $\eta^{(2)}$ given by (17) the maximum eigenvalues of $(\eta^{(2)})^2$ yielding

$$d = J^2\sqrt{16\alpha^2(\eta_{21}^2 + \eta_{22}^2) + \eta_{23}^2 + \mathcal{O}(\tau_p^5)}. \quad (18)$$

In this formula, the quadratic dependence of d as a function of J has been put in evidence. The quadratic dependence on τ_p is less manifest, but it becomes obvious on inspecting the integrals in (8) from which $\eta_{2j} = \mathcal{O}(\tau_p^2)$ ensues.

Once τ_s and $v(t)$ are known, the coefficients η_{21} , η_{22} , and η_{23} can be easily computed according to (8). Thereby, we have an analytical prediction for the leading order of d as function of J including the prefactor. For fixed value of J , Eq. (18) as a function of α is characterized by a constant behaviour dominated by η_{23} for $\alpha \ll 1$ and a linear behaviour in α for large values of the coupling constant.

B. The Range of Parameters

Although we are focusing here on the theoretical issues it is helpful to have an idea about the experimental range of parameters. In the sequel, we thus try to assess the relevant ranges. The numbers given represent only crude estimates since the precise values depend strongly on the particular experimental setup. Moreover, the relevant decoherence processes are not yet always known.

First, we consider liquid NMR like crotonic acid or alanine [28]. The pulse lengths τ_p used are in the range of

200 μ s. The maximum pulse amplitude B_m for a π pulse is thus in the range of 10kHz. The couplings between the nuclear spins lie between 1 and about 70 Hz. A key ratio is J/B_m , i.e., the relative dimensionless strength of the pulse. Here it takes values in the range of 10^{-4} and 10^{-2} . The other important parameter α is the dimensionless ratio ω_b/λ between the internal energy scale ω_b of the bath and the coupling between qubit and bath. Because the coupling between the switched spin is typically of the same order as the coupling between the other spins α is roughly of the order of 1.

Second, we consider a solid NMR system, namely KPF₆. There, we found $B_m \approx 90$ kHz and interspin couplings ranging from 3.3kHz to 11kHz [29]. This implies $J/B_m \approx 0.04 - 0.12$ whereas α ranges between 0.3 and 3. Another system is adamantane, for which we assume $B_m \approx 150$ kHz and $J \approx 15$ kHz so that $J/B_m \approx 0.1$. The ratio α is again taken to be of the order of 1 [30].

Third, we consider the electronic spin in a quantum dot as the qubit. The experimental investigation of temperature dependent spin relaxation has just started [31]. The pulses are very short ($\tau_p \approx 1$ ps) which implies for a π pulse according to $B_m\tau_p/\hbar = \Theta/2 = \pi/2$ the amplitude $B_m \approx 1$ meV. But it is much less clear which λ or α one should consider. In Ref. 31 a bosonic bath with spectral density $J_{\text{eff}}(\omega)$ is considered. Taking the Debye frequency $\omega_D = 27.5$ meV as upper cutoff and deducing J from

$$J^2 = \int_0^{\omega_D} J_{\text{eff}}(\omega)d\omega \quad (19)$$

one obtains $J \approx 0.3 - 20$ eV which implies enormous values for J/B_m but small values for $\alpha = \omega_D/J$.

But closer inspection of the estimates for T_2 [31] reveals that the above estimate is not the relevant one. Rather the internal energy scale appears to be set by the energy splitting $\Delta \approx 70\mu$ eV of the two qubit states. The characteristic coupling is found by restricting the integral in (19) to the interval $[0, \Delta]$. Then $J \approx 1 - 6$ eV ensues which implies $J/B_m \approx 10^{-6} - 10^{-5}$ and $\alpha \approx 10^4$. Hernandez et al. [31] doubt the relevance of the spin relaxation via Rashba and Dresselhaus terms advocating phonon-induced dephasing [32, 33]. Then one should rather estimate $J^2 \approx \Gamma\Delta$ with $\Gamma \approx 0.2\mu$ eV implying $J \approx 4\mu$ eV. Then $J/B_m \approx 0.004$ and $\alpha \approx 20$. This example illustrates that the unambiguous identification of the relevant processes of decoherence is still a challenging task.

Fourth, we consider a qubit realized by charge states in a superconducting device [34]. The pulse length is $\tau_p \approx 80$ ps implying $B_m \approx 15\mu$ eV. The coupling J is taken from the free decay $J \approx \hbar/150$ ps $\approx 5\mu$ eV while we deduce $\omega_b \approx 0.2\mu$ eV from the decay of the signal with an echo pulse. So $J/B_m \approx 0.3$ and $\alpha \approx 0.04$.

Fifth and last, we look at trapped ions [35] for which we found pulse lengths in the range of microseconds implying $B_m \approx 1$ MHz. The coupling to optical modes takes values $J \approx 20 - 200$ kHz so that $J/B_m \approx 0.02 - 0.2$. Less

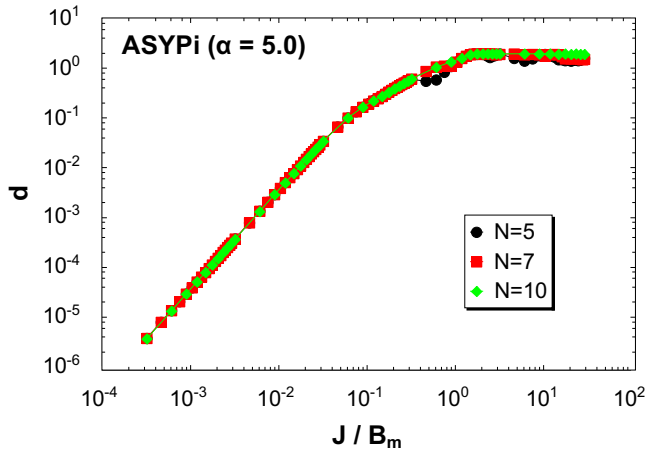


Figure 5: (Color online) Deviation d as a function of J/B_m (B_m is the maximum amplitude of the pulse) for various lengths N of the spin chain at $\alpha = 5.0$. The data refers to the ASY1 pulse.

obvious is the relevant internal energy scale ω_b . The energies of the optical modes in the cavities are fairly high between 1 and 40GHz so that α would range in the order of 10^6 . Thus the question arises whether this is really the relevant scale or whether the very fast modes average out so that a much lower effective scale comes into play.

The above numbers provide a rough guideline in which range today's experiments are done. Surely, more elaborate investigations of the relevant decoherence mechanisms are called for.

IV. THE NUMERICAL ANALYSIS

Remarks on the program The numerical data was obtained using C++ routines. Many of the matrix calculations were realized with the help of the MATPACK-package [36]. The exponentials of the matrices were calculated using routines adapted from EXPOKIT [37] abbreviated `padm`. These are techniques based on Padé summation. Note that this approach is well-suited to deal with piecewise constant pulses whereas continuously varying pulses are not accessible.

As anticipated from the analytical calculation, only minor finite-size effects occur. This is illustrated numerically in Fig. 5 for one particular pulse. But all other pulses show the same behavior. Indeed, the finite-size effects are completely negligible in the region of small values of J . Hence we conclude that a moderate number of bath spins is sufficient. In the data presented here we routinely use $N = 7$ and $N = 10$. For these system sizes no particular matrix algorithms are needed.

π pulses: vanishing linear order We consider symmetric and asymmetric pulses with angle $\theta = \pi$ which satisfy $\eta_{11} = \eta_{12} = 0$ as defined in (8). For comparison,

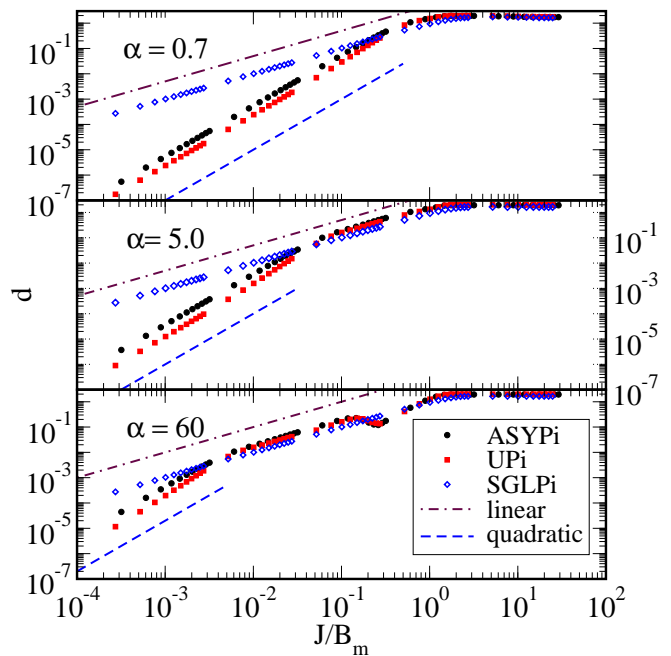


Figure 6: (Color online) Case of π pulses. The deviation d is plotted as function of J/B_m for $N = 10$ and various values of α . For an unbiased comparison of the pulses, J is normalized to the maximum amplitude B_m of the pulses. The notation for the pulses refers to Tab. I. The dashed lines ease the comparison with pure power laws.

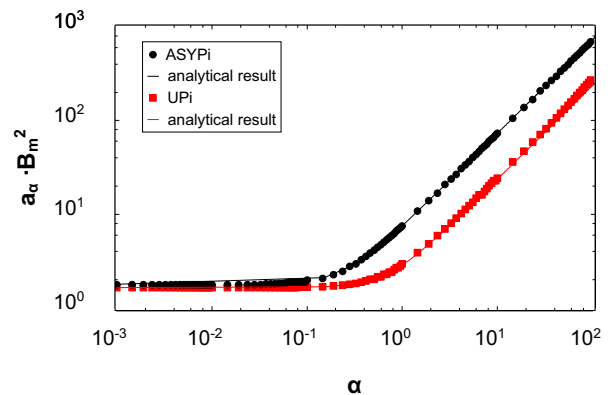


Figure 7: (Color online) Case of π pulses. Plot of the prefactors a_α in $d = a_\alpha J^2 + \mathcal{O}(J^3)$ for $N = 7$. The solid lines represent the analytical prediction in Eq. (18).

also the standard pulse with constant amplitude and finite $\eta^{(1)}$ is computed.

Fig. 6 shows the behavior of the deviations d as a function of J/B_m for representative values of the parameter α . Here B_m is the maximum amplitude of the pulse. At first thought, a plot as function of $J\tau_p$ appears reasonable. But the comparison as function of J/B_m is fairer because the simple pulses, for instance the standard one

SGLPi, need only a smaller amplitude. Hence they can experimentally be realized with a shorter duration τ_p if the apparatus restricts the maximum applicable amplitude. This advantage is accounted for by the plot versus J/B_m .

The quadratic behavior of ASYPi and UPi proves that the first order corrections are completely cancelled. This is not the case for SGLPi for which the numerical data display a linear behavior for small J . For large values of α , d starts to deviate from the desired quadratic behavior even at relative small values of J . This indicates that the internal energy scale $\omega_b = \alpha J$ becomes important.

The comparison between the standard pulse SGLPi and the optimized ones ASYPi and UPi shows that a crossover takes place. For low values of J the pulses with vanishing first order outperform the standard pulse due to their steeper decrease. At larger values of J the more complicated structure of the optimized pulses does not pay anymore and SGLPi is slightly better. Note that the value of J where the crossover takes place depends on the value of α . For low values of α ASYPi and UPi pay up to much larger values of J than for large values of α .

Data such as presented in Fig. 6 is used to determine the prefactors a_α defined in

$$d = a_\alpha J^2 + \mathcal{O}(J^3) \quad (20)$$

by fits. The fits are made only within the range of validity of the quadratic behavior. The results are plotted in Fig. 7. They agree perfectly with the analytical prediction from Eq. (18). For the quantitative comparison the coefficients η_{21} , η_{22} , and η_{23} are explicitly computed for ASYPi and UPi2 by means of Eqs. (8), see also Tab. I.

$\pi/2$ pulses: vanishing linear order We consider symmetric and asymmetric pulses with angle $\theta = \pi/2$ which satisfy $\eta_{11} = \eta_{12} = 0$ as defined in (8). For comparison, also the standard pulse with constant amplitude and finite $\eta^{(1)}$ is computed.

Fig. 8 shows the behavior of the deviations d as a function of J/B_m for representative values of the parameter α . Again, the comparison as function of J/B_m is fairer for the above mentioned reasons.

The quadratic behavior of ASYPi2 and UPi2 proves that the first order corrections are completely cancelled. This is not the case for SGLPi2 for which the numerical data displays a linear behavior for small J . For large values of α , d starts to deviate from the desired quadratic behavior even at relative small values of J . This indicates that the internal energy scale $\omega_b = \alpha J$ becomes important.

The comparison between the standard pulse SGLPi2 and the optimized ones ASYPi2 and UPi2 shows that a crossover takes place. For low values of J the pulses with vanishing first order outperform the standard pulse due to their steeper decrease. At larger values of J the more complicated structure of the optimized pulses does not pay anymore and SGLPi2 is slightly better. Note that the value of J where the crossover takes place depends on the value of α . For low values of α ASYPi2 and UPi2

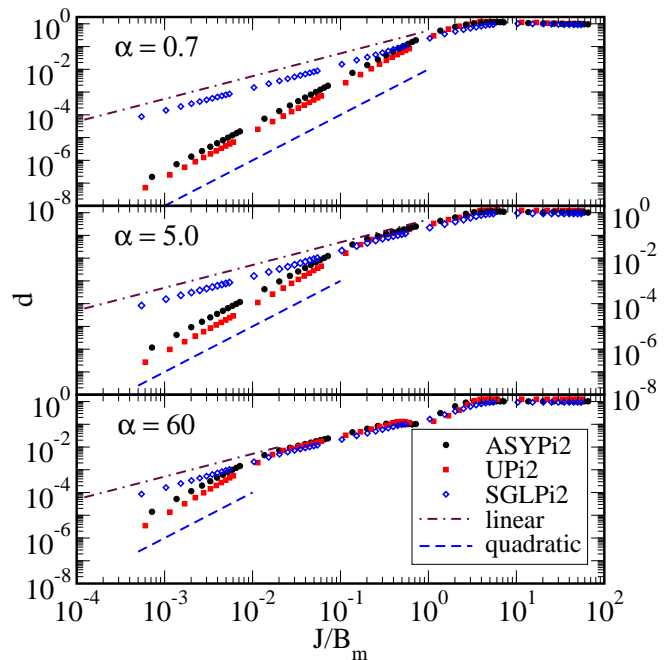


Figure 8: (Color online) Case of $\pi/2$ pulses. The deviation d is plotted as function of J/B_m for $N = 10$ and various values of α . For an unbiased comparison of the pulses, J is normalized to the maximum amplitude B_m of the pulses. The notation for the pulses refers to Tab. II. The dashed lines ease the comparison with pure power laws.

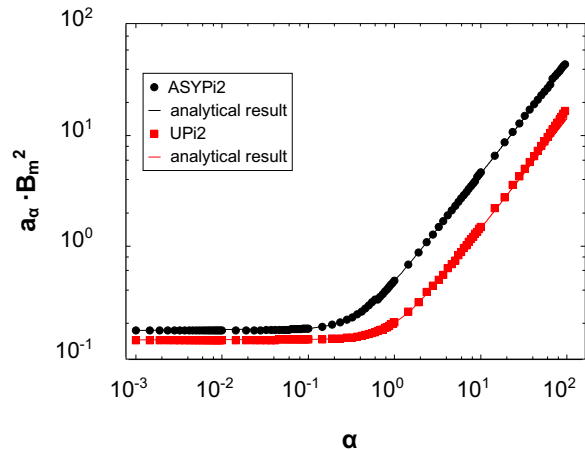


Figure 9: (Color online) Case of $\pi/2$ pulses. Plot of the prefactors a_α in $d = a_\alpha J^2 + \mathcal{O}(J^3)$ for $N = 7$. The solid lines represent the analytical prediction in Eq. (18).

pay up to much larger values of J than for large values of α .

Note that the gain of the optimized pulses over the standard pulse is most significant for low values of α , i.e., for a slow internal bath dynamics. It is less significant for fast internal bath dynamics corresponding to large values

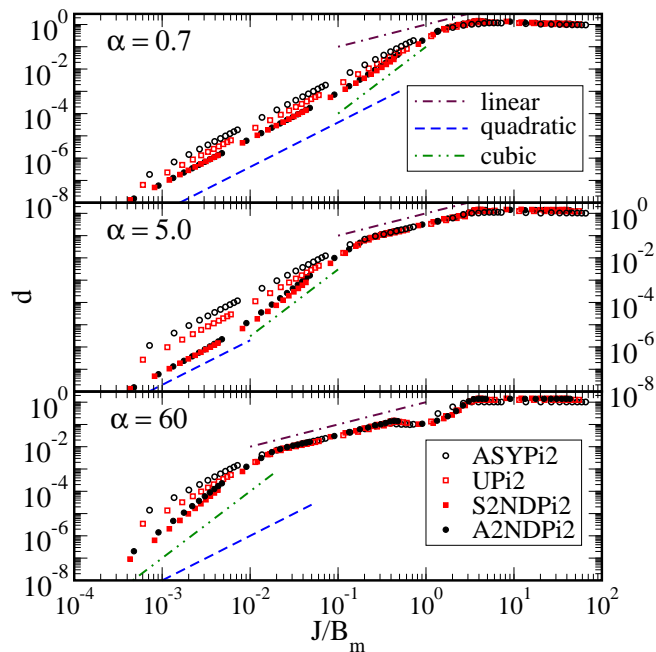


Figure 10: (Color online) Case of $\pi/2$ pulses with partly vanishing quadratic order. The deviation d is plotted as function of J/B_m for $N = 10$ and various values of α . For an unbiased comparison of the pulses, J is normalized to the maximum amplitude B_m of the pulses. The notation for the pulses refers to Tab. II. The dashed lines ease the comparison with pure power laws.

of α .

Data such as presented in Fig. 8 is used to determine the prefactors a_α defined in (20) by fits. The fits are made only within the range of validity of the quadratic behavior. The results are plotted in Fig. 9. They agree perfectly with the analytical prediction in Eq. (18). For the quantitative comparison the coefficients η_{21} , η_{22} , and η_{23} are explicitly computed for ASYPi2 and UPi2 by means of Eqs. (8), see also Tab. II.

The errors in the fits of the prefactors for the $\pi/2$ pulses were determined by hand for some randomly chosen data points using various fitting ranges and fitting functions such as $bJ + a_\alpha J^2$ or $a_\alpha J^2 + bJ^3$. This analysis provides the error estimates of 12% at $\alpha = 0.03$ to 32% at $\alpha = 28$ for pulse UPi2 and about 10% for all α looking at pulse ASYPi2.

$\pi/2$ pulses: partly vanishing quadratic order In the previous work in Refs. [20] we have proven rigorously that no π pulse can satisfy the second order Eqs. (8c,8d,8e). For $\pi/2$ pulses no such proof is known to us. But we were not able to find a solution to all five equations Eqs. (8) either.

We managed, however, to find solutions which make the first four equations (8a,8b,8c,8d) vanish. The advantage is that the first order vanishes completely and that in second order all the terms of order $\lambda\omega_b\tau_p^2$ vanish also. Only the term of order $\lambda^2\tau_p^2$ persists. We expect such

pulses, see Fig. 3 and Tab. II, to be advantageous for systems where the coupling λ between qubit and bath is very small, but the internal bath dynamics ω_b is not.

Here we propose two possible examples of $\pi/2$ pulses, symmetric and asymmetric, for which $\eta_{11} = \eta_{12} = 0$, $\eta_{21} = \eta_{22} = 0$, but $\eta_{23} \neq 0$. From the above arguments, we expect that for large values of α , i.e., fairly fast baths, the deviation $d(J)$ displays cubic behavior at least in some intermediate range. Fig. 10 provides the corresponding data. Indeed, one clearly identifies an intermediate range where cubic behavior is seen. This range is fairly small for small values of α (upper panel in Fig. 10) but grows upon increasing α (middle panel in Fig. 10). For the large values of α analyzed in the lower panel in Fig. 10 the quadratic behavior below the cubic range is not even discernible. But we know from Eq. (18) that it exists.

We conclude that even a partial vanishing of the second order can be very helpful. This conclusion is supported by the comparison to data for ASYPi2 and UPi2 which have a vanishing first order, but no vanishing second order terms. As to be expected, we find that for low values of J the pulses S2NDPi2 and A2NDPi2 outperform ASYPi2 and UPi2. For larger values of J a crossover takes place and there is no need to resort to the more complicated pulses S2NDPi2 and A2NDPi2. There, all pulses behave very much alike.

Note that the crossover takes place for lower values of J if α is large and viceversa for larger values of J if α is small. This is related to the fact that the range of cubic behavior occurs at larger values of J for small α . For large α the range is larger, but shifted to smaller values of J .

V. CONCLUSIONS

We numerically simulated the effect of designed short control pulses on a qubit coupled to a bath of spins. The effect of the short pulse can be approximated in leading order of the pulse duration τ_p as a δ peak. For finite τ_p , however, corrections occur which we know from previous analytical calculations. The aim of the present work was two-fold. First, we wanted to confirm the analytical results by numerical calculations. Second, we intended to analyze to which extent the analytically neglected higher orders matter. Put differently, we wanted to see whether pulses, which are fine-tuned to make the leading corrections vanish, outperform the standard pulses.

The numerical results confirm the analytical results in all points. The fine-tuned pulses display qualitatively different power laws in the deviation d as function of $J\tau_p$. This deviation measures the difference between the ideal pulse, multiplied with the evolution due to free decoherence, and the realistic pulse. For standard pulses, one has $d \propto J$. For the fine-tuned pulses we achieve $d \propto J^2$.

In restricted parameter ranges, we obtained even $d \propto J^3$ for pulses which make certain parts of the second order

corrections vanish. Such pulses were not yet discussed before. They are only possible for $\theta \neq \pi$.

The second goal has also been achieved by the analysis of the real performance in case of the coupling to a spin bath. We could show that the fine-tuned pulses outperform the more standard ones in a large range of parameters. Furthermore, we estimated the relevant parameters for a number of generic experiments. These estimates show that many experimental setups are such that the fine-tuned pulses should improve on the standard pulses. But more investigations, both theoretical and experimental, are needed to obtain a complete understanding of the important decoherence mechanisms.

For the above reasons we suggest that the choice of

the optimized pulses with respect to the standard ones is in many cases preferable. Our findings here will provide guidelines under which experimental circumstances one should use the optimized pulses.

Acknowledgments

We would like to thank M. Bayer, T. Fischer, A. Greilich, M. Lovrić, and J. Stolze for helpful discussions. The financial support in GK 726 by the DFG is gratefully acknowledged.

-
- [1] L. Viola and S. Lloyd, Phys. Rev. A **58**, 2733 (1998).
 - [2] M. Ban, J. Mod. Opt. **45**, 2315 (1998).
 - [3] P. Facchi, S. Tasaki, S. Pascazio, H. Nakazato, A. Tokuse, and D. A. Lidar, Phys. Rev. A **71**, 022302 (2005).
 - [4] P. Cappellaro, J. S. Hodges, T. F. Havel, and D. G. Cory, J. Chem. Phys. **125**, 044514 (2006).
 - [5] W. M. Witzel and S. DasSarma, Phys. Rev. Lett. **98**, 077601 (2007).
 - [6] W. Yao, R. B. Liu, and L. J. Sham, Phys. Rev. Lett. **98**, 077602 (2007).
 - [7] G. S. Uhrig, Phys. Rev. Lett. **98**, 100504 (2007).
 - [8] U. Haeberlen, *High Resolution NMR in Solids: Selective Averaging* (Academic Press, New York, 1976).
 - [9] L. M. K. Vandersypen and I. L. Chuang, Rev. Mod. Phys. **76**, 1037 (2004).
 - [10] E. L. Hahn, Phys. Rev. **80**, 580 (1950).
 - [11] H. Y. Carr and E. M. Purcell, Phys. Rev. **94**, 630 (1954).
 - [12] S. Meiboom and D. Gill, Rev. Sci. Inst. **29**, 688 (1958).
 - [13] K. Khodjasteh and D. A. Lidar, Phys. Rev. Lett. **95**, 180501 (2005).
 - [14] K. Khodjasteh and D. A. Lidar, Phys. Rev. A **75**, 062310 (2007).
 - [15] G. S. Uhrig, New J. Phys. **10**, 083024 (2008).
 - [16] J. J. L. Morton, A. M. Tyryshkin, A. Ardavan, S. C. Benjamin, K. Porfyarakis, S. A. Lyon, and G. A. D. Briggs, Nature Phys. **2**, 40 (2006).
 - [17] J. R. Petta, A. C. Johnson, J. M. Taylor, E. A. Laird, A. Yacoby, M. D. Lukin, C. M. Markus, M. P. Hanson, and A. C. Gossard, Science **309**, 2180 (2005).
 - [18] A. Greilich, R. Oulton, E. A. Zkukov, I. A. Yugova, D. R. Yakovlev, M. Bayer, A. Shabaev, A. L. Efros, I. A. Merkulov, V. Stavarache, et al., Phys. Rev. Lett. **96**, 227401 (2006).
 - [19] B. Lee, W. M. Witzel, and S. DasSarma, Phys. Rev. Lett. **100**, 160505 (2008).
 - [20] S. Pasini, T. Fischer, P. Karbach, and G. S. Uhrig, Phys. Rev. A **77**, 032315 (2008). S. Pasini and G. S. Uhrig, J. Phys. A:Math. Theor. **41**, 312005 (2008).
 - [21] R. Tycko, Phys. Rev. Lett. **51**, 775 (1983).
 - [22] H. Geen and R. Freeman, J. Mag. Res. **93**, 93 (1991).
 - [23] H. K. Cummins and J. A. Jones, New J. Phys. **2**, 6 (2000).
 - [24] H. K. Cummins, G. Llewellyn, and J. A. Jones, Phys. Rev. A **67**, 042308 (2003).
 - [25] P. Chen, C. Piermarocchi, and L. J. Sham, Phys. Rev. Lett. **87**, 067401 (2001).
 - [26] D. A. Garanin and R. Schilling, Europhys. Lett. **59**, 7 (2002).
 - [27] M. Möttönen, R. de Sousa, J. Zhang, and K. B. Whaley, Phys. Rev. A **73**, 022332 (2006).
 - [28] E. M. Fortunato, M. A. Pravia, N. Boulant, G. Teklemariam, T. F. Havel, and D. G. Cory, J. Chem. Phys. **116**, 7599 (2002).
 - [29] M. Lovrić, H. G. Krojanski, and D. Suter, Phys. Rev. A **75**, 042305 (2007).
 - [30] M. Lovrić, private communication (2008).
 - [31] F. G. G. Hernandez, A. Greilich, F. Brito, M. Wiemann, D. R. Yakovlev, D. Reuter, A. D. Wieck, and M. Bayer, Phys. Rev. B **78**, 041303(R) (2008).
 - [32] Y. G. Semenov and K. W. Kim, Phys. Rev. Lett. **92**, 026601 (2004).
 - [33] Y. G. Semenov and K. W. Kim, Phys. Rev. B **75**, 195342 (2007).
 - [34] Y. Nakamura, Y. A. Pashkin, T. Yamamoto, and J. S. Tsai, Phys. Rev. Lett. **88**, 047901 (2002).
 - [35] D. Leibfried, R. Blatt, C. Monroe, and D. Wineland, Rev. Mod. Phys. **75**, 281 (2003).
 - [36] B. M. Gammel, *Matpack version 1.9.0*, www.matpack.de (2006).
 - [37] R. B. Sidje, ACM Trans. Math. Softw. **24**, 130 (1998).